Boundary-layer method for the analytical calculation of stable textures of bent-core liquid crystal fibers

Román Pérez-Ortiz,[1] Orlando Guzmán,[1] and J. Adrián Reyes[1,2]
[1]*Departamento de Física, Universidad Autónoma Metropolitana, Iztapalapa, Apdo 55 534, México DF, 09340, México*
[2]*On leave from Instituto de Física, UNAM*
(Received 21 March 2011; published 5 July 2011)

We study the equilibrium textures of molecular orientation inside cylindrical fibers made of coaxial layers of bent-core smectics. We propose a free-energy model taking into account surface-like and bulk contributions—including layer-compression and electrostatic terms among others— with constant values of the material parameters. We follow the usual variational procedure of minimization of the free energy with respect to the tilt-angle profile $\theta(r)$ and obtain an Euler-Lagrange equation and its boundary condition. We solve the variational equations for the equilibrium configurations using a boundary-layer approximation and find multiple solutions. Since the equilibrium tilt profiles are found to be radially inhomogeneous, we select those with minimum distortions in order to find the lowest free-energy state. We minimize further the free energy of the system with respect to the fiber radius and find wider intervals of stability than those previously reported, depending on the balance of the material's spontaneous polarization, elastic and electric divergence-of-polarization constants, and surface-tension coefficients. The bulk and surface-layer structures thus found could be used to calculate the allowed modes of propagation of electromagnetic waves inside the fiber.

DOI: 10.1103/PhysRevE.84.011701 PACS number(s): 61.30.Dk, 61.30.Pq, 64.70.Nd

I. INTRODUCTION

Low-molecular weight liquid crystals may form fibers depending on the type of mesogen and phase: their columnar phases can produce slender fibers, but the smectic and nematic phases of the calamitic type cannot [1,2]. Bent-core smectics have been used to produce bundles of fibers drawn from phases B_2 and B_7 [3,4]. Their internal structure was determined to be constituted by multilayered, helical fibers [5]. Characterization of the helical filaments shows that they are composed of cylindrical coaxial smectic layers [6,7]. More recently, Bailey and coworkers have analyzed the elastic properties, internal structure, and stability of fiber bundles for five bent-core systems, using a variety of experimental techniques [8]. They found that the individual fibers fuse together in filaments with enlarged radii, compared to those of the isolated ones.

Bent-core liquid crystals are interesting for applications in optoelectronics because they can spontaneously form fibers with internal nanostructure. In addition, the presence of well-aligned molecular dipoles in each smectic layer introduces the possibility of differential propagation of circularly polarized light, that is, biased conduction of electromagnetic waves [9]. In fact, Jákli *et al.* have carried out experiments to show that these fibers perform like optical waveguides [10].

It would be useful to have mathematical models of the structure of bent-core liquid crystal fibers that could be applied, in turn, to model the electromagnetic properties of such systems. Bailey and coworkers presented a model for the free energy of individual fibers that accounts for director and molecular-dipole distortions, layer strain, electrostatic interactions, and surface tension [11]. They analyzed the stability of fibers by minimizing this free-energy model with respect to the radius of the fiber, assuming that the tilt angle that defines the molecular orientation is constant through all layers.

Bauman and Philips have presented a generalization of the model of Bailey *et al.* for B_7 fibers that includes general (noncircular) cross-sections [12]. Their model includes an energy density for the layers in terms of the complex order parameter for smectics, ψ. They were able to deduce a limiting model by assuming a layer width much smaller than the fiber radius, and then freezing both molecular tilt angles (leaving the director and polarization fields **n** and **p** with one degree of freedom). Using this limiting energy, they showed that circular fibers are stable if the layer bending constant $a_\perp \simeq K$, the Frank elastic modulus. Conversely, If K is much smaller than $a_\perp$, they show that circular fibers are unstable with respect to variations having surface undulations and modulations of the component of the polarization along the layer plane.

The requirement of homogeneous orientation in the liquid crystal is a very restrictive hypothesis when compared with other treatments of mesophases, where the director field is the quantity to vary in order to minimize the free energy. Hence, we reconsider this problem by lifting the restriction of constant director tilt and minimize the free energy using standard calculus-of-variation techniques.

We propose revised expressions for the bulk and surface free-energy terms, appropriate for inhomogeneous tilt, and use a boundary-layer method in order to solve analytically the associated Euler-Lagrange and boundary-condition equations. We find multiple radially dependent solutions, which nevertheless become uniform away from a boundary layer near the cylinder border. We pick those solutions with minimum distortions in order to find the lowest-free-energy structures and then minimize again their free energy with respect to the fiber outer radius in order to identify the stable size of the fibers. We discuss the conditions on the elastic, electrostatic, and surface-tension terms that result in stable fibers. We compare our results with those obtained previously using the constant-tilt model of Bailey *et al.* [11] and observe wider intervals of stability.

Finally, we comment on extensions of this approach to the case where the molecular-dipole orientation α is not constant as well as possible applications of our results.

 ©2011 American Physical Society

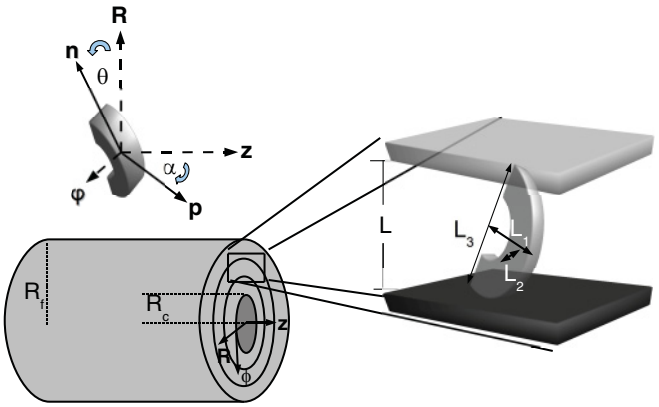

FIG. 1. (Color online) Structure of the smectic layers in the fiber, showing the coordinate system (R,ϕ,z). The external radius of the fiber is R_f and the radius of its inner defect core is R_c. The width L of each layer depends on the dimensions L_1, L_2, and L_3 of a single mesogen as well as the molecular orientation: θ is the angle between the director $\mathbf{n}$ and the radial direction; α is the angle between $\mathbf{p}$ and the z axis.

II. FREE-ENERGY MODEL

Our model follows that presented by Bailey and coworkers for the case of homogeneous orientation [11]; in order to facilitate comparisons with that case, we adopt most of the notation introduced in that model. We consider the simple fiber structure shown in Fig. 1: a cylindrical fiber with external radius R_f is composed by coaxial smectic layers. Near the center of the fiber, we assume that there is a defect core of size $R_c \ll R_f$; the results of the analysis are independent of R_c and the energy associated with this core [11].

We take into account five contributions to the Helmholtz free-energy density of a bent-core smectic fiber: elastic distortions of the director, layer compression, divergence of polarization, electrostatic dipole interaction, and surface tension. To describe these contributions, we use a molecular basis formed by the director $\mathbf{n}$, the molecular-dipole vector $\mathbf{p}$, and $\mathbf{m} = \mathbf{n} \times \mathbf{p}$, and introduce cylindrical coordinates (R,ϕ,z).

We assume that $\mathbf{n}$ is confined to planes normal to the fiber axis, with a radially dependent tilt $\theta(R)$; we also assume a constant molecular-dipole orientation α (see Fig. 1). The molecular basis is parametrized as:

$$\mathbf{n} = \cos\theta\hat{\mathbf{R}} + \sin\theta\hat{\boldsymbol{\varphi}}, \tag{1}$$

$$\mathbf{p} = \sin\theta\sin\alpha\hat{\mathbf{R}} - \cos\theta\sin\alpha\hat{\boldsymbol{\varphi}} + \cos\alpha\hat{\mathbf{z}}, \tag{2}$$

$$\mathbf{m} = \sin\theta\cos\alpha\hat{\mathbf{R}} - \cos\theta\cos\alpha\hat{\boldsymbol{\varphi}} - \sin\alpha\hat{\mathbf{z}}. \tag{3}$$

In this parametrization, the director is always perpendicular to the fiber's axis but with the possibility of tilting away from the radial direction. The tilt angle $\theta = 0$ corresponds to a director that is along the radial direction (that is, normal to the smectic layers and the surface of the fiber), while $\theta = \pi/2$ corresponds to the director perpendicular to the radial direction. On the other hand, angle $\alpha = 0$ corresponds to molecular dipoles pointing along the fiber's longitudinal axis, while $\alpha = \pm\pi/2$ corresponds to molecular dipoles perpendicular to said axis.

We restrict θ and α to the interval $[-\pi/2,\pi/2]$ because these values cover all posible orientations of the director and molecular-dipole vector (relative to the fiber's axis and its external-surface tangent and normal vectors).

A. Director distortions

Macroscopic distortions of the director contribute to the bulk free-energy density with a term [13,14]

$$F_N = \frac{K}{2}[(\nabla\cdot\mathbf{n})^2 + (\nabla\times\mathbf{n})^2] = \frac{K}{2}\left[\frac{1}{R^2} + \left(\frac{\mathrm{d}\theta}{\mathrm{d}R}\right)^2\right], \tag{4}$$

where K is the elastic modulus in the one-constant approximation. Saddle-splay and splay-bend terms are not included in the model: the former vanishes identically; the latter is neglected because little is known experimentally about the effective value of K_{13} [15–18] and also because even if it were as large as K, we estimate that the splay-bend contribution to the total free energy would be negligible compared to other surface contributions that we discuss below.

B. Layer compression

Changes in angle θ imply changes in layer spacing. We account for this with a harmonic layer-compression term in the bulk free-energy density [13,14],

$$F_C = \frac{B\gamma^2}{2} = \frac{B}{2}\left(\frac{L - L_0}{L_0}\right)^2, \tag{5}$$

where B is the compression modulus and γ is the layer strain due to variations of the layer thickness L from that of its equilibrium value L_0.

We approximate L in the following way: we take a parallelepiped that encloses a single mesogen; the edges of the parallelepiped are given by vectors $\mathbf{L}_1$, $\mathbf{L}_2$, and $\mathbf{L}_3$. The magnitudes L_1, L_2, and L_3 of these vectors are given, respectively, by the molecular dimensions along the medium, short, and long axes of the mesogen, and their orientations change with the orientation of the mesogen. Then the layer width, as a function of θ and α, is given by the distance between two parallel planes that touch the highest and lowest corners of the parallelepiped. Since one can go from the lowest corner to the highest one along three edges of the parallelogram, the distance between those planes can be calculated from three projections of the edges onto the radial direction, $\mathbf{L}_i \cdot \hat{\mathbf{R}}$:

$$L(\theta,\alpha) = L_3|\cos\theta| + L_2|\cos\alpha\sin\theta| + L_1|\sin\alpha\sin\theta|. \tag{6}$$

The absolute values are necessary to pick the correct high and low corners as the angles θ and α change sign.

Other approximations are possible for the layer width, such as using ellipsoids instead of parallelepipeds or introducing diagonal shape tensors [11]. We must point out, however, that all these approximations, including Eq. (6), neglect that d is not an even function of α nor θ due to the bent-core character of the mesogens. Nevertheless, since the mesogens are relatively slender (see Table I for typical mesogen parameters), we do

TABLE I. Constant values of the material parameters for the examples discussed in this work. The values are taken from the intervals given in Ref. [11].

Symbol	Value	Description
R_c	5.0 nm	Core radius
K	10^{-11} N	Elastic constant
B	10^5 Pa	Layer compression modulus
L_3	5.0 nm	Long axis of mesogens
L_2	0.5 nm	Short axis of mesogens
L_1	1.5 nm	Medium axis of mesogens
α_0	0	Orientation of **p** in strain-free layers
P_0	10^{-4} C m^{-2}	Norm of spontaneous polarization
ϵ_1	7	Dielectric constant along **n**
ϵ_2	10	Dielectric constant along **m**
ϵ_3	12	Dielectric constant along **p**
c''	11.2 V	Electric div.-of-polarization const.
σ_1	0.026 N m^{-1}	Surface tension along **n**
σ_2	0.024 N m^{-1}	Surface tension along **m**
σ_3	0.025 N m^{-1}	Surface tension along **p**

not expect qualitative changes in the results as one changes from one of these approximations to another.

With the approximation given in Eq. (6), the layer-compression term becomes

$$f_c = \frac{B}{2}\left[\frac{d(\theta,\alpha)}{d_0} - 1\right]^2, \tag{7}$$

with the dimensionless thickness

$$d(\theta,\alpha) = \frac{L(\theta,\alpha)}{L_3}, \tag{8}$$

and the strain-free thickness $d_0 = d(\theta_0,\alpha_0)$ parametrized by the angles θ_0 and α_0.

C. Electrostatic energy of anisotropic dielectric

In bent-core smectics, the electric displacement field

$$\mathbf{D} = \mathbf{P}_s + \epsilon_0 \overleftrightarrow{\epsilon} \cdot \mathbf{E} \tag{9}$$

depends both on the spontaneous polarization $\mathbf{P}_s$ and the dielectric tensor $\overleftrightarrow{\epsilon} = \epsilon_1\mathbf{nn} + \epsilon_2\mathbf{mm} + \epsilon_3\mathbf{pp}$. Constants ϵ_1,ϵ_2, and ϵ_3 are the eigenvalues of the dielectric tensor corresponding to the molecular-frame eigenvectors **n**,**m**, and **p**.

The free-energy density of dielectrics obeying the constitutive relation (9) has been discussed by Landau, Lifshitz, and Pitaevskii; it is given by [19]

$$F_E = \tfrac{1}{2}\epsilon_0 \mathbf{E} \cdot \overleftrightarrow{\epsilon} \mathbf{E}, \tag{10}$$

for processes that take place at fixed charges, temperature, and density.

Using $\nabla \times \mathbf{E} = 0$ over a circular path of radius R inside the fiber, we conclude that **E** is radial. Next, following Bailey and coworkers [11], we assume that $\mathbf{P}_s = P_0\mathbf{p}$; in other words, that the spontaneous polarization is aligned with the molecular-dipole vector **p** and has constant magnitude P_0. Then, from $\nabla \cdot \mathbf{D} = 0$ and the constitutive relation we find that

$$\mathbf{E} = -\frac{P_0 \sin\alpha}{\epsilon_0 \epsilon_{rr}(\theta)}\left(\sin\theta - \frac{R_c}{R}\sin\theta_c\right)\hat{\mathbf{R}}, \tag{11}$$

where θ_c is the tilt angle at the fiber's core and

$$\epsilon_{rr}(\theta) = \epsilon_1 \cos^2\theta + (\epsilon_2 \cos^2\alpha + \epsilon_3 \sin^2\alpha)\sin^2\theta.$$

Substitution of the electric field just found into Eq. (10) gives the free-energy density as:

$$F_E = \frac{1}{2}\frac{P_0^2 \sin^2\alpha}{\epsilon_0 \epsilon_{rr}(\theta)}\left(\sin\theta - \frac{R_c}{R}\sin\theta_c\right)^2. \tag{12}$$

D. Inhomogeneities of the molecular-dipole vector and polarization

Distortions of the molecular-dipole vector contribute to the bulk free-energy density as $c'\nabla \cdot \mathbf{p}$ and those of the spontaneous polarization contribute with $c''\nabla \cdot \mathbf{P}_s$. Using again the assumption $\mathbf{P}_s = P_0\mathbf{p}$, both terms can be combined and integrated to obtain a single contribution to the surface free-energy density:

$$F_D = (c' + c''P_0)\mathbf{p} \cdot \hat{\mathbf{R}} = (c' + c''P_0)\sin\alpha \sin\theta. \tag{13}$$

E. Interfacial energy

Assuming a biaxial form of the interfacial-energy tensor,

$$\overleftrightarrow{\sigma} = \sigma_1\mathbf{nn} + \sigma_2\mathbf{mm} + \sigma_3\mathbf{pp}, \tag{14}$$

the free-energy density for the cylindrical surface of the fiber is

$$F_S = \hat{\mathbf{R}} \cdot \overleftrightarrow{\sigma} \cdot \hat{\mathbf{R}} = \sigma_1 \cos^2\theta + (\sigma_2 \cos^2\alpha + \sigma_3 \sin^2\alpha)\sin^2\theta. \tag{15}$$

F. Dimensionless total free energy

Integrating all contributions discussed above, the total free energy of the fiber is

$$F_{\text{tot}} = \int_0^{L_z}\int_0^{2\pi}\left[(F_D + F_S)R_f + \int_{R_c}^{R_f}(F_N + F_E + F_C)R\,\mathrm{d}R\right]\mathrm{d}\varphi\,\mathrm{d}z. \tag{16}$$

We introduce a scaled radial coordinate $r = R/R_f$, the scaled radius of the core $r_c = R_c/R_f$, and the notation $\dot{\theta} = \frac{\mathrm{d}\theta}{\mathrm{d}r}$. Then we define a dimensionless total free energy as

$$f_{\text{tot}} = \frac{F_{\text{tot}}}{2\pi L_z K} = f_{\text{surf}} + \int_{r_c}^{1} f_{\text{bulk}}\mathrm{d}r, \tag{17}$$

where L_z is the length of the fiber. In Eq. (17), the dimensionless surface free-energy density is

$$f_{\text{surf}}(\theta) = \frac{R_F}{K}(F_D + F_S) = A_D f_D(\theta) + A_S f_S(\theta), \tag{18}$$

and the corresponding bulk density is

$$f_{\text{bulk}}(\theta,\dot{\theta}) = \frac{R\,R_f}{K}(F_N + F_C + F_E) = r\left\{\frac{1}{2}\left[\dot{\theta}^2 + \frac{1}{r^2}\right] + A_C f_C(\theta) + A_E f_E(\theta)\right\}, \tag{19}$$

with contributions given by

$$f_D(\theta) = \sin\alpha \sin\theta \tag{20}$$

$$f_S(\theta) = \cos^2\theta + \left(\frac{\sigma_2}{\sigma_1}\cos^2\alpha + \frac{\sigma_3}{\sigma_1}\sin^2\alpha\right)\sin^2\theta, \tag{21}$$

$$f_C(\theta) = \frac{1}{2}\left(\frac{d(\theta,\alpha)}{d_0} - 1\right)^2, \tag{22}$$

$$f_E(\theta) = \frac{1}{2}\frac{\sin^2\alpha}{\epsilon_{rr}(\theta)}\left(\sin\theta - \frac{r_c}{r}\sin\theta_c\right)^2, \tag{23}$$

and the dimensionless parameters

$$A_D = (c' + c''P_0)R_f/K, \tag{24}$$

$$A_S = \sigma_1 R_f/K, \tag{25}$$

$$A_C = BR_f^2/K, \tag{26}$$

$$A_E = P_0^2 R_f^2/(\epsilon_0 K). \tag{27}$$

III. VARIATIONAL CONDITIONS FOR FREE-ENERGY MINIMIZATION

Thermodynamic equilibrium requires that the tilt configuration $\theta(r)$ minimizes the total free energy f_{tot}. Bailey *et al.* assumed a constant tilt profile over the whole bulk of the fiber in order to perform this minimization [11].

Instead, we assume that $\theta(r)$ is subject to variations, with a fixed value $\theta(r_c) = \theta_c$ at the core of the fiber and a free value $\theta(1) = \theta_1$ at the cylinder surface. This corresponds in variational calculus to the problem of finding an extremal of $f_{\text{tot}}(\theta,\dot{\theta})$ with one endpoint fixed and a second one free [20]. Hence, the variational conditions to be met are the Euler-Lagrange equation in the bulk,

$$\frac{\partial f_{\text{bulk}}}{\partial\theta} - \frac{\mathrm{d}}{\mathrm{d}r}\left\{\frac{\partial f_{\text{bulk}}}{\partial\dot{\theta}}\right\} = 0, \tag{28}$$

and the boundary condition

$$\left[\frac{\mathrm{d}f_{\text{surf}}}{\mathrm{d}\theta} + \frac{\partial f_{\text{bulk}}}{\partial\dot{\theta}}\right]_{r=1} = 0 \tag{29}$$

at the cylinder surface. Satisfying these conditions corresponds to solving the ordinary differential equation

$$\frac{\mathrm{d}}{\mathrm{d}r}\left(r\frac{\mathrm{d}\theta}{\mathrm{d}r}\right) - r\left(A_C\frac{\partial f_C}{\partial\theta} + A_E\frac{\partial f_E}{\partial\theta}\right) = 0, \tag{30}$$

subject to the boundary condition

$$\dot{\theta}(1) + \left[A_D\frac{\partial f_D}{\partial\theta} + A_S\frac{\partial f_S}{\partial\theta}\right]_{r=1} = 0. \tag{31}$$

Notice that, in general, a uniform tilt profile $\theta(r) = \theta_1$ that satisfies the boundary condition will not satisfy the Euler-Lagrange equation and vice versa. For instance, take the case where the direction of the molecular dipole $\alpha = \pi/2$: the boundary condition of Eq. (31) reduces to

$$\sin\theta_1 = \frac{A_E}{2A_S(\sigma_3/\sigma_1 - 1)} = \frac{c' + c''P_0}{\sigma_3 - \sigma_1}.$$

Solutions to this equation exists only for particular combinations of the spontaneous polarization P_0, the interfacial energies σ_i, and divergence-of-polarization constants c' and c''. Most likely, the uniform profiles corresponding to these solutions will not solve the Euler-Lagrange equation because that condition involves other parameters: the elastic constant K and the layer-compression modulus B.

Therefore, in the next section we look for nonuniform tilt profiles as solutions to the variational equations, aware that such solutions may exist only for particular sets of material parameters.

IV. ANALYTICAL SOLUTIONS TO THE VARIATIONAL CONDITIONS

A. Relative magnitude of the bulk free-energy densities

The relative size of the coefficients in the Euler-Lagrange equation gives insight on the solutions: the layer-compression energy will dominate over the electrostatic contribution if their coefficients satisfy that $A_C > A_E$, that is, when

$$\sqrt{\epsilon_0 B} > P_0. \tag{32}$$

In order to illustrate our calculations with a concrete example, let us consider the case of a system with material parameters given in Table I; these constant parameter values are within the intervals of reasonable values for real systems—set out by Bailey and coworkers [11]. We will keep as variables the remaining parameters of the model (namely α, θ_0, c', and R_f).

In our example, $P_0 < \sqrt{\epsilon_0 B} \approx 10^{-3}\mathrm{C\,m^{-2}}$, and the layer-compression energy dominates over the electrostatic term. On the contrary, the electrostatic energy f_E would be the governing interaction if we had P_0 much larger than $\sqrt{\epsilon_0 B}$. As in most materials, the spontaneous polarization is expected to be rather small [19], this would not occur often. We will examine the former limit first and discuss the latter one at the end of this section.

For the values specified in Table I, the ratio $A_E/A_C = 0.0113$ is rather small; therefore, we can consider the electrostatic contribution given by f_E as a small perturbation. This will simplify greatly our problem.

What characteristic distance, δ, is required for the change of θ, such that the elastic term becomes comparable to the layer-compression term in Eq. (30)? The answer is found by approximating the derivative $\frac{\mathrm{d}}{\mathrm{d}r}$ as $\frac{1}{\delta/R_f}$. Then we find that δ corresponds to characteristic distance for smectics $\delta = \sqrt{K/B}$; in our example $\delta = 10\mathrm{nm}$. The experimentally observed radius of the fibers is on the order of one to several microns [4] and so we will have that $\delta \ll R_f$. This means that we will find generally that the layer-compression coefficient $A_C = BR_f^2/K = (R_f/\delta)^2$ is large compared with unity, besides being large compared with A_E.

Such a small characteristic distance for the variation of θ suggests looking for solutions that are constant almost everywhere over the bulk of the fiber, except for a thin layer near its surface [21]. Then, in order to satisfy the Euler-Lagrange equation away from the boundary layer, the value of θ in the bulk of the fiber must be any of the roots of

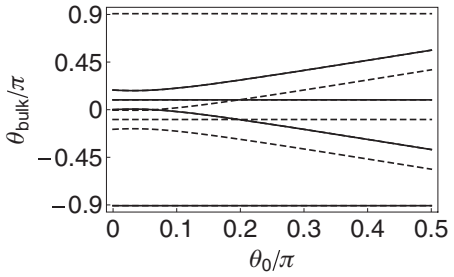

FIG. 2. Roots of the function $g(\theta)$ that determine the possible values of the tilt angle in the bulk, $\theta_{\rm bulk}$, as a function of the tilt angle in strain-free layers, θ_0. Solid lines correspond to the molecular-dipole orientation $\alpha = \pi/2$; dashed ones to $\alpha = -\pi/2$. These two sets are symmetrical under the reflection $\theta_{\rm bulk} \leftrightarrow -\theta_{\rm bulk}$.

the function $g(\theta)$, defined by

$$g(\theta) = \frac{\partial f_C}{\partial \theta} + \lambda \frac{\partial f_E}{\partial \theta} = 0, \tag{33}$$

where the perturbation parameter $\lambda = A_E/A_C$ is much smaller than unity.

Multiple roots $\theta_{\rm bulk}$ solving Eq. (33) can be found numerically or estimated analytically (as perturbations of the roots of the dominant layer-compression term). The roots for our example are shown in Fig. 2 for the cases with $\alpha = \pm\pi/2$, as functions of the parameter θ_0 that defines the strain-free layer configuration. In that figure, there are eight different branches of solutions of Eq. (33). Four of these solutions correspond to the value $\alpha = \pi/2$ and the other four to the case $\alpha = -\pi/2$. For each of these two groups of solutions, we find two branches that are independent of θ_0 and two more that do vary with it.

Each of the branches shown in Fig. 2 may give rise to different solutions to the entire variational problem. Therefore, we investigate next how to find boundary-layer solutions to the Euler-Lagrange and boundary condition equations [21], assuming that far from the fiber surface the solution becomes practically constant, that is,

$$\lim_{r \to r_c} \theta(r) = \theta_{\rm bulk}. \tag{34}$$

B. Boundary-layer solutions

As we expect the tilt angle to vary rapidly with r in a boundary layer, we change to a new coordinate t defined by

$$r = \exp(t/\sqrt{A_C}). \tag{35}$$

Multiplying both sides of Eq. (30) by r, and noticing that $r\frac{\rm d}{{\rm d}r} = \sqrt{A_C}\frac{\rm d}{{\rm d}t}$, the Euler-Lagrange equation becomes

$$\frac{{\rm d}^2\theta}{{\rm d}t^2} - e^{2t/\sqrt{A_C}}\left(\frac{\partial f_C}{\partial \theta} + \lambda \frac{\partial f_E}{\partial \theta}\right) = 0. \tag{36}$$

Nevertheless, the exponential factor in the latter equation can be approximated as unity, because we have assumed that A_C is very large. Recalling Eq. (33), the Euler-Lagrange equation simplifies to

$$\frac{{\rm d}^2\theta}{{\rm d}t^2} - g(\theta) = 0. \tag{37}$$

The solution of this differential equation can be sought in terms of special functions or by numerical methods; however, we can gain significant insight if we approximate the equation and find solutions in terms of elementary functions. Even if we may lose some precision, the situation is analogous to representing a simple pendulum by a harmonic oscillator, because the general behavior will be illuminated by the analytically soluble model.

For that reason, we expand $g(\theta)$ in a Taylor series around one of its roots $\theta_{\rm bulk}$ and truncate to the first order in $\Delta\theta = \theta - \theta_{\rm bulk}$:

$$\frac{{\rm d}^2\Delta\theta}{{\rm d}t^2} - k\Delta\theta = 0, \tag{38}$$

where $k = g'(\theta_{\rm bulk})$. Solving Eq. (38), we find

$$\theta(r) = \theta_{\rm bulk} + C_1 r^{\sqrt{kA_C}} + C_2 \frac{1}{r^{\sqrt{kA_C}}}. \tag{39}$$

The sign of k governs the behavior of the solution at the fiber's core and external boundary. Negative k leads to rapid and undamped oscillatory behavior near the fiber's core, which lacks the required uniform limit, $\lim_{r\to r_c}\theta(r) = \theta_{\rm bulk}$. Cases with $k = 0$ amount to constant tilt angle; we have shown already that this type of profile does not satisfy generally the external-boundary condition. Only for positive $k = g'(\theta_{\rm bulk})$ we can guarantee that $\theta(r)$ goes to its bulk value as $r \to r_c$, by choosing $C_2 = 0$. This reduces the number of suitable roots of $g(\theta)$ that can serve as values of $\theta_{\rm bulk}$.

An analysis of the sign of k reveals that in the example of Fig. 2, the constant branches have negative slope, while the nonconstant branches have positive slopes and therefore positive k. Thus, we need only to consider further the nonconstant branches to develop our boundary-layer solutions.

When $k > 0$, the tilt profile is simply

$$\theta(r) = \theta_{\rm bulk} + (\theta_1 - \theta_{\rm bulk}) r^{\sqrt{kA_C}}, \tag{40}$$

where we recognize that $C_1 = \theta_1 - \theta_{\rm bulk}$ corresponds to the difference between the tilt angle at the external boundary and at the fiber's core.

We can determine C_1 or, equivalently, θ_1 using the external-boundary condition that reduces to

$$(\theta_1 - \theta_{\rm bulk})\sqrt{kA_C} + \left[A_S \frac{\partial f_S}{\partial \theta} + A_D \frac{\partial f_D}{\partial \theta}\right]_{\theta=\theta_1} = 0.$$

Explicitly, we need to solve for θ_1 the equation

$$(\theta_1 - \theta_{\rm bulk})\sqrt{kA_C} = A_S \sin(2\theta_1)\left(\frac{\sigma_1 - \sigma_2}{\sigma_1} + \frac{\sigma_2 - \sigma_3}{\sigma_1}\sin^2\alpha\right) - A_D \sin\alpha\cos\theta_1. \tag{41}$$

If we plot each side of Eq. (41) versus θ_1, we find that the left-hand one is a straight line, while the other is an oscillatory function. The values of θ_1 that solve the boundary condition are given by the intersections of these two curves; they can be found graphically or numerically. Figure 3 shows that multiple intersections may exist, depending on the values of the parameters of the liquid crystal fiber. Each value of θ_1 at the intersections gives rise to a different solution for the tilt profile.

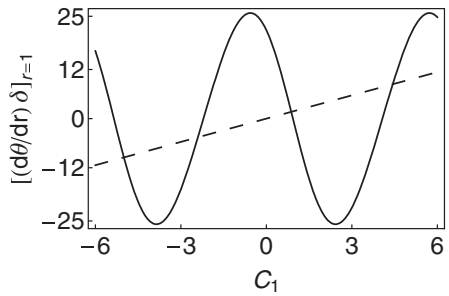

FIG. 3. Determination of the constant $C_1 = \theta(1) - \theta_{\text{bulk}}$ as the intersection of the left- and right-hand sides in the boundary condition, Eq. (41). Solutions with larger values of C_1 are expected to have larger distortions and therefore larger free energies.

Larger values of $C_1 = \theta_1 - \theta_{\text{bulk}}$ imply larger distortions of the director, so they result in higher values of the elastic free energy. Since we are interested in the stable configurations of the fiber, we need to analyze only solutions that correspond to intersections with small values of C_1. For instance, in Fig. 3, $C_1 = -2.38$ and $C_1 = 0.76$ give the smallest tilt-angle change between the core and the exterior of the fiber; both values correspond to the same physical situation because we do not distinguish between θ and $\theta \pm \pi$. In the rest of the paper we concentrate only on such low-C_1 solutions (that correspond to the smallest tilt distortions), because we expect solutions with higher values of C_1 to be metastable or unstable with respect to the former ones.

Examples of solutions $\theta(r)$ in the form of Eq. (40), found with the method just described, are shown in Fig. 4. As expected, the solutions consist of two regions: one where θ is practically constant and another of rapid spatial variation near the border of the fiber. The width of the boundary layer corresponds to the formerly introduced distance $\delta = \sqrt{K/B}$.

The presence of this boundary layer, characterized by a rapid spatial variation, is a consequence of the boundary condition at the cylindrical border, Eq. (31). This is a hybrid boundary condition or first-order differential equation, which, as explained in Section III, cannot be generally satisfied by a constant solution to the Euler-Lagrange Eq. (30) in the bulk. Therefore, the boundary layer allows matching of said boundary condition with a practically homogeneous solution deep inside the fiber, and we expect this type of behavior independently of the approximation used for the layer width,

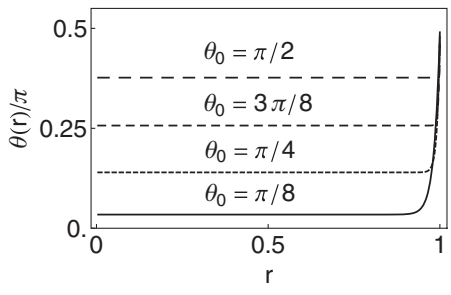

FIG. 4. Boundary-layer profiles for the tilt angle $\theta(r)$ as functions of the radial coordinate r, satisfying the Euler-Lagrange equation and boundary condition, for different values of the tilt angle in strain-free layers, θ_0. The width of the boundary layer is given by $\delta = \sqrt{K/B}$.

$d(\theta,\alpha)$. It should be stressed that, in spite of having constant tilt inside the fiber's bulk, these solutions exhibit indeed a lot of splay distortion around the defect core, which is consistent with the presence of said defect.

These boundary-layer configurations minimize the total free energy for a fixed radius R_f, but we would like to find which radii are the most stable ones by further minimizing the free energy with respect to R_f. We take up this task in the next section.

Before going to that, we point out that if the dominant term in the bulk free-energy density were the electrostatic energy, we could in principle reverse the roles of A_E and A_C, and then repeat the analysis given above: we would define then $\tilde{g}(\theta) = f_E(\theta) + \tilde{\lambda} f_C(\theta)$, with the perturbation parameter $\tilde{\lambda} = A_C/A_E$. Next, we would search for boundary-layer solutions of the form $\theta(r) = \theta_{\text{bulk}} + C_1 r^{\sqrt{kA_E}}$, fix the values of θ_{bulk} as roots of $\tilde{g}(\theta)$, and find C_1 by solving the external-boundary condition. Of course, one would have to pick only those values θ_{bulk} that lead to positive values of $k = \tilde{g}'(\theta)$.

V. STABLE RADIUS OF THE FIBER

The reduced free energy f_{tot} of a fiber can be calculated as a function of its radius R_f by substituting into Eq. (17) the boundary-layer profiles $\theta(r)$ found in the previous section.

We evaluated analytically both surface-like terms as well as the elastic bulk-energy density. Nevertheless, we had to integrate numerically the layer-compression and electrostatic bulk-energy densities. Because of the rapid variation of the tilt-angle in the boundary layer, it was useful to perform the integration over the variable t, defined in Eq. (35), instead of the coordinate r. Thus, we can calculate the total free energy for a fiber with a given set of material parameters.

We concentrate now on the dependence of the reduced free energy $f_{\text{tot}}(R_f,\theta_0)$ with respect to the fiber radius, at a given value of the tilt in strain-free smectic layers (θ_0), keeping all other material parameters constant. The bottom panel in Fig. 5 illustrates this function for the case with $\theta_0 = 1$. The location of a minimum in such function reveals the radius of stable fibers, the ones that minimize the free energy with respect to both R_f and the tilt profile $\theta(r)$. In the example given in Fig. 5, the radius of stable fibers is $R_{\text{min}} = 3.08\,\mu$m.

When will the total free energy display such minima with respect to the fiber radius? The answer lies in the competition among different contributions to the free energy. Inspection of Eqs. (19)–(23) shows that all of the free-energy densities are positive-definite, except the surface-like divergence-of-polarization term. Only when this term is negative and comparable to the sum of the other terms, we expect the presence of minima in the total free energy; otherwise the minimum of the free energy corresponds to null radius, i.e., the absence of fibers.

We can estimate values of the material parameters that lead to minima in f_{tot}. For instance, assume that the electrostatic coefficient A_E is indeed smaller than the layer-compression coefficient A_C, that is, $P_0^2/\epsilon_0 < B$. Then, the surface-tension coefficient A_S will dominate over both A_C and A_E if the surface-tension coefficient $\sigma_1 > BR_f$; for typical values $\sigma \sim 10^{-2}$ N/m and $B \sim 10^5$ Pa, this will be true when the radius of the fiber is larger than 0.1 μm. In that case, in

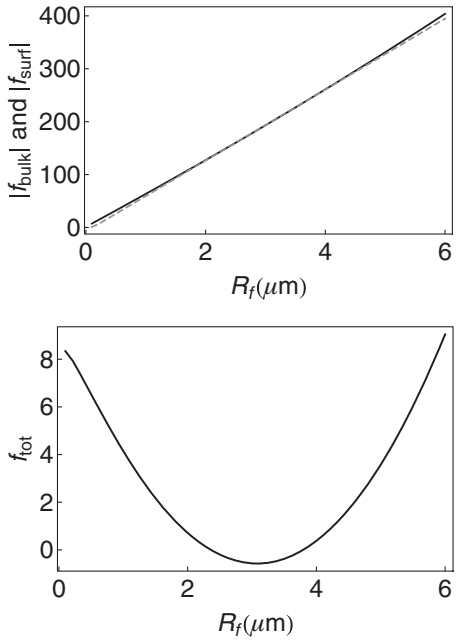

FIG. 5. The absolute value of the bulk and surface-like contributions to the free energy are of the same order of magnitude (top panel: solid and dashed lines, respectively, for the case $\theta_0 = 1$), but the former is positive-definite while the latter may be negative. Therefore, in some cases, their competition gives rise to minima in the total free energy with respect to the fiber radius R_f. When minima exist (bottom panel), their location $R_{\min}$ corresponds to the radius of stable fibers for the given value of the strain-free angle θ_0.

order to have minima and stable fibers, we require that the divergence-of-polarization coefficient A_D is negative and of the same order of magnitude or larger than the surface-tension term, A_S. This will happen when $\sin\alpha$ and $\sin\theta$ have opposite signs and

$$c' + c'' P_0 > \sigma_1. \tag{42}$$

This can be achieved with a high value of c' independently of the spontaneous polarization (when $c' > \sigma_1$) or, conversely, with a sufficiently high value of the spontaneous polarization P_0 (when $c' < \sigma_1$). The top panel in Fig. 5 illustrates this competition: although the two surface-like terms are much larger than the individual contributions of the bulk terms, their sum is of the same order as that of the combined bulk terms. Since the total surface-like energy is still negative, it competes with the positive bulk energy and produces the minimum shown in the bottom panel of Fig. 5.

The converse situation, where the divergence-of-polarization term competes with the layer-compression term, would introduce the condition

$$c' + c'' P_0 > B R_f. \tag{43}$$

This condition requires again sufficiently high values of c' and P_0, because in practice it is not possible to decrease arbitrarily the value of R_f below a critical limit $R_{\text{critical}} \approx 0.15\mu$m, set by a modified Plateau-Rayleigh instability [4] (that fragments a fluid cylinder into a set of disconnected droplets).

In order to illustrate the effect of changes in the material parameters, we have calculated the stable radius $R_{\min}(\theta_0, c')$

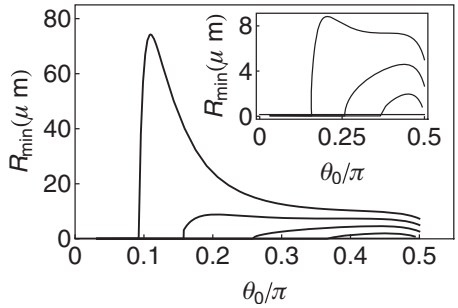

FIG. 6. Stable radii of fibers as functions of the tilt angle in strain-free layers, θ_0, for different values of the elastic divergence-of-polarization constant, c'. The main panel, from bottom to top, shows results for $c' = 0.0245, 0.0246, 0.0247$, and $0.0248\,\text{N m}^{-1}$. The inset shows a zoom to the curves for the three smallest values of c'. In all four cases, a gap devoid of stable fibers is observed for values of θ_0 close to zero; its width decreases with increasing c'.

as a function of the tilt in strain-free layers, θ_0, for the values $c' = 0.0245, 0.0246, 0.0247$, and $0.0248\,\text{N m}^{-1}$, taking all other material parameters as in Table I. The results are shown in Fig. 6.

We report the following results: first, no stable fibers are found unless θ_0 exceeds a minimum value, creating a forbidden region or gap of instability around $\theta_0 = 0$. Second, this minimum value shifts toward zero as c' is increased, which reduces the width of the gap. Finally, the stable fibers become markedly thicker as the constant c' rises above the value of the surface-tension eigenvalues, encompassing the experimentally measured sizes of fibers drawn from B_2 and B_7 phases [4,11]. As a matter of fact, if c' becomes a few percent larger than the surface tension coefficients, we find that the radius of the fiber grows to tens of microns.

The results shown in Fig. 6 can be compared directly with those of Bailey *et al.* for constant profiles $\theta(r) = \theta_{\text{bulk}}$, in particular with Fig. 7 in Ref. [11]. The calculations for a constant-tilt profile indicate that the radius of stable fibers does not change more than one order of magnitude as the spontaneous polarization changes over three orders of magnitude. Also, in addition to the gap of instability near $\theta_0 = 0$, for constant-tilt profiles there is a second gap of instability near $\theta_0 = \pi/2$.

Thus, our results for the boundary-layer solutions coincide with the previous finding of Bailey and coworkers that there is a gap of instability at values of θ_0 close to zero, where no stable fibers can be found. By contrast, while the radius of stable fibers with boundary-layer solutions does decrease near $\theta_0 = \pi/2$, we do not observe a second instability gap near that value: we still find stable radii different from zero. Also differently for the case of constant tilt, we find stable fibers with radius as large as tens of microns, when a negative divergence of polarization energy overcomes the positive surface-tension energy and compete with the bulk energy of the fiber.

We attribute these differences to the very important role played by the surface-like terms in our model; this role is set by the rapid variation of the tilt angle required in our model in order to satisfy the boundary conditions, which couple the solution in the bulk with the surface-like energy densities.

VI. CONCLUSIONS

We presented a revised model for the free energy of fibers made from smectic layers of bent-core mesogens. This model does not assume that the tilt-angle profile $\theta(r)$ is constant throughout the bulk of the fiber; instead, we use such a model to identify those profiles $\theta(r)$ that minimize the free-energy functional $f_{\text{tot}}[\theta(r)]$.

The standard procedures of variational calculus were applied to obtain the Euler-Lagrange equation for $\theta(r)$ and its associated boundary condition at the external surface of the fiber. Then we identified the dominant contributions to the free energy and developed an approximate, analytical solution to the variational equations. The solutions display a boundary-layer behavior: the profile $\theta(r)$ is nearly constant but for a thin layer near the external surface of the fiber. The width of the boundary layer is set by the characteristic length for perturbations in smectic layers, $\delta = \sqrt{K/B}$; for typical values of the material parameters, this length is of the order of tens of nanometers.

Numerical integration of the bulk free-energy densities reveals that, for a given value of the strain-free tilt θ_0, the free-energy function f_{tot} can be minimized with respect to the fiber's radius R_f; such minima correspond to the radius of stable fibers. The existence of said minima depends sensitively on the competition of the total surface-like energy and the total bulk energy. The divergence-of-polarization term is very important because it is the only one that can be negative and compete with the other terms (which are positive-definite).

Another feature of our model with variable-tilt profiles is that the instability gap—or interval of absence of stable fibers observed for values of θ_0 close to zero—becomes smaller as the elastic divergence-of-polarization constant c' is increased even slightly above the values of the surface-tension coefficients σ_i. Large values of the radius of stable fibers are found even for small spontaneous polarizations, on the order of 10^{-4} C m^{-2}. At any rate, the model is able to recover radius of stable fibers that are compatible with those reported experimentally for fibers drawn from both B_2 and B_7 phases.

We conjecture that the high values that the surface-like energy terms can acquire in our model may give a hint to the aggregation of fibers into compact bundles: although our present model cannot address currently this issue, it may be possible that a modified version of the model can take into account the interaction of several fibers in close proximity, and to figure out whether they can reduce their combined surface-like energy by bundling, as found experimentally by Bailey *et al.* [8].

Another modification to the model that strikes us as worthy of consideration is that of allowing variations of the molecular-dipole angle α, so that the free energy could be minimized simultaneously with respect to $\alpha(r)$ and $\theta(r)$. In addition to this, we think it would be interesting to incorporate into the model the smectic layer energy in terms of the complex order parameter ψ, as presented by Bauman and Phillips [12]. We expect that the boundary-layer method will be useful for those cases, too.

Finally, examination of the conditions of propagation of right- and left-circularly polarized light within fibers with nonuniform tilt angle profiles would be of interest in the context of optical applications. Particularly, the effect of the boundary layer and its associated and rapid variation of the dielectric tensor near the external surface of the fiber could imply interesting phenomena of transmission and reflection at the air-liquid crystal interface.

ACKNOWLEDGMENTS

O. Guzmán acknowledges support from Programa de Mejoramiento del Profesorado (PROMEP) of the Secretaría de Educación Pública, México.

[1] M. P. Mahajan, M. Tsige, P. L. Taylor, and C. Rosenblatt, Liq. Cryst. **26**, 443 (1999).
[2] D. H. Van Winkle and N. A. Clark, Phys. Rev. Lett. **48**, 1407 (1982).
[3] G. Pelzl, S. Diele, A. Jákli, C. H. Lischka, I. Wirth, and W. Weissflog, Liq. Cryst. **26**, 135 (1999).
[4] A. Jákli, D. Krüerke, and G. G. Nair, Phys. Rev. E **67**, 051702 (2003).
[5] G. Liao, S. Stojadinovic, G. Pelzl, W. Weissflog, S. Sprunt, and A. Jákli, Phys. Rev. E **72**, 021710 (2005).
[6] A. Jákli, C. Lischka, W. Weissflog, G. Pelzl, and A. Saupe, Liq. Cryst. **27**, 1405 (2000).
[7] C. Bailey and A. Jákli, Phys. Rev. Lett. **99**, 207801 (2007).
[8] C. Bailey, M. Murphy, A. Eremin, W. Weissflog, and A. Jákli, Phys. Rev. E **81**, 031708 (2010).
[9] L. O. Palomares, P. Castro-Garay, and J. A. Reyes, Appl. Phys. Lett. **94**, 181903 (2009).
[10] J. Fontana, C. Bailey, W. Weissflog, I. Jánossy, and A. Jákli, Phys. Rev. E **80**, 032701 (2009).
[11] C. Bailey, E. C. Gartland, and A. Jákli, Phys. Rev. E **75**, 031701 (2007).
[12] P. Bauman, and D. Phillips, Mol. Cryst. Liq. Cryst. **510**, 1 (2009).
[13] P. de Gennes and J. Proust, *The Physics of Liquid Crystals* (Clarendon Press, Oxford, 1993).
[14] R. Holyst and A. Poniewierski, J. Phys. II **3**, 177 (1993).
[15] H. Yokoyama, Phys. Rev. E **55**, 2938 (1997).
[16] M. Faetti and S. Faetti, Phys. Rev. E **57**, 6741 (1998).
[17] M. Kleman and O. D. Lavrentovich, *Soft Matter: An Introduction* (Springer, New York, 2003).
[18] A. Ferrarini, Liq. Cryst. **37**, 811 (2010).
[19] L. D. Landau, E. M. Lifshitz, and L. P. Pitaevskii, *Electrodynamics of Continuous Media* (Butterworth-Heinemann, London, 1984), 2nd ed.
[20] J. L. Troutman, *Variational Calculus and Optimal Control* (Springer, New York, 1996), 2nd ed.
[21] C. M. Bender and M. C. Arszog, *Advanced Mathematical Methods for Scientists and Engineers* (McGraw-Hill, New York, 1978).